# ARTEC: Accelerated Reconstruction of High Angular Resolution Diffusion Imaging with Trajectory Error Correction

Ashutosh Vaish[1,*], Anubha Gupta[1], and Ajit Rajwade[2]

[1]SBILab, Department of ECE, IIIT-Delhi, India
[2]Department of CSE, IIT-Bombay, India
Email: ashutoshv@iiitd.ac.in (A.V.); anubha@iiitd.ac.in (A.G.); ajitvr@cse.iitb.ac.in (A.R.)
[*]Corresponding author
Manuscript received June 12, 2024; revised January 10, 2025; accepted January 14, 2025; published March 17, 2025

***Abstract*—Diffusion Magnetic Resonance Imaging (dMRI) is being increasingly used to study neural connectivity of brain regions. High Angular Resolution Diffusion Imaging (HARDI) reliably estimates the local orientations of white matter tracts for neural connectivity analysis in the brain. However, HARDI suffers from long acquisition times, limiting its clinical usage. An effective way to reduce the acquisition time is to acquire an undersampled signal followed by its compressive reconstruction. In general, due to various calibration inaccuracies in the MR scanners, acquisition trajectories in the *k*-space get perturbed. Although radial sampling allows significant undersampling, the trajectory errors are more pronounced with it. Hence, if the trajectory errors are not corrected, compressive reconstruction of the signal would be adversely impacted. In this work, we propose ARTEC, a joint framework of accelerated reconstruction of the HARDI signal undersampled in the joint (*k*-*q*)-space, while incorporating trajectory error corrections. Simulation results on both phantom and real data demonstrate the superior performance of the proposed method over the existing state-of-the-art methods.**

***Keywords*—Diffusion MRI, HARDI compressed sensing, trajectory errors, Spherical Ridgelets**

## I. Introduction

Diffusion Magnetic Resonance Imaging (dMRI) is an imaging modality for analyzing white matter integrity and neural connectivity among brain regions. dMRI is captured as a set of MR images individually acquired in the *k*-space by applying different diffusion gradients specified by the *b*-vector and *b*-value, together defining the *q*-space [1]. Thus, dMRI is 4D data, where each sample in the *q*-space represents a 3D MRI volume. High Angular Resolution Diffusion Imaging (HARDI), a popular variant of dMRI, is good at distinguishing closely aligned nerve fiber tracks in a voxel but suffers from long acquisition times. This is inconvenient to patients and makes the scanning error-prone. Hence, compressive sensing (CS) based accelerated reconstruction is increasingly being used in HARDI to reduce the acquisition time [2, 3].

Although Cartesian sampling is used prominently for the acquisition of dMRI, radial sampling is also becoming popular due to its added advantages. Firstly, in the radial sampling, each radial spoke samples the whole span of low and high-frequency information, making it less sensitive to motion artifacts. Secondly, the sampling pattern due to radial is inherently dense at low-frequency regions that allows the image to be reconstructed using fewer projections producing comparatively less pronounced aliasing due to undersampling [4, 5].

Despite the above-mentioned benefits, radial trajectories are affected by perturbations due to hardware imperfections like eddy currents and gradient timing errors, wherein the signal is acquired at *k*-space frequencies that differ from the specified or nominal frequencies ($\mathbf{u}$) [6]. Since the frequency encoding gradients are different for each spoke in radial sampling, a different erroneous shift or perturbation $\boldsymbol{\delta_i}$ is introduced in the $i^{th}$ spoke. This substantially reduces the quality of the image, especially in the case of accelerated reconstruction. However, the image recovery can be improved to a great extent if these frequency perturbations are known, allowing to reconstruct the signal using the actual or perturbed frequencies $\mathbf{u} + \mathbf{v}$, where $\mathbf{v}$ are the perturbations in frequencies. Also, since each radial line is perturbed as a whole, perturbation of all the points on a radial line can be modeled using a value of the trajectory perturbation $\boldsymbol{\delta}_i$ in the $i^{th}$ spoke. Recently, a few trajectory correction methods have been proposed for radial sampling in MRI by the detection of the erroneous shifts [6, 7]. Inspired by the above discussion, we propose a novel joint method for recovery of perturbations ($\boldsymbol{\delta}$) in the nominal frequencies ($\mathbf{u}$) along with the recovery of HARDI image ($\boldsymbol{X}$) from the undersampled *k*-space measurements.

## II. Method

A HARDI data is a 4D volume of size $s_x \times s_y \times s_z \times d$, where $s_x \times s_y$ denotes the size of one MR slice, $s_z$ denotes the number of slices in a volume, and $d$ denotes the number of gradient directions. HARDI can also be seen as a collection of $d$ MRI volumes (in *k*-space), where each MRI volume is captured with a different diffusion gradient (specified by a *b*-vector and a *b*-value in *q*-space). Henceforth, we resize the HARDI data as a 2D matrix, $\boldsymbol{X} = [\boldsymbol{x}_1\, \boldsymbol{x}_2 \ldots \boldsymbol{x}_v]^T \in \mathbb{R}^{v \times d}$ where $v = s_x \times s_y \times s_z$ is the number of voxels and $\boldsymbol{x}_i \in \mathbb{R}^d$ is the diffusion gradient signal at the $i^{th}$ voxel.

### A. Subsampling

For subsampling in *q*-space, we selected $r_q$ samples using the operator $\boldsymbol{\Phi}_q \in \mathbb{R}^{r_q \times d}$ from the available $d$ no. of *q*-space samples over the spherical shell, using the quasi-uniform random sampling scheme [8]. Similarly, for *k*-space subsampling, we chose $r_k$ voxels using $\boldsymbol{\Phi}_k \in \mathbb{R}^{r_k \times v}$ by selecting uniformly distributed radial lines in the *k*-space. We use the radial sampling with alignment $\boldsymbol{\theta} \in [0, \pi]$. Further, for a joint (*k*-*q*) space subsampling, the *q*-space and *k*-space

sampling operators $\boldsymbol{\Phi}_k$ and $\boldsymbol{\Phi}_q$ are used as $\boldsymbol{\Phi}_{k,q}\boldsymbol{X} = \boldsymbol{\Phi}_k \boldsymbol{X} \boldsymbol{\Phi}_q^{\mathrm{T}}$ to select a total of $r_k \times r_q$ samples, where $\boldsymbol{\Phi}_{k,q} = \boldsymbol{\Phi}_q \otimes \boldsymbol{\Phi}_k \in \mathbb{R}^{r_k r_q \times vd}$ using the Kronecker product.

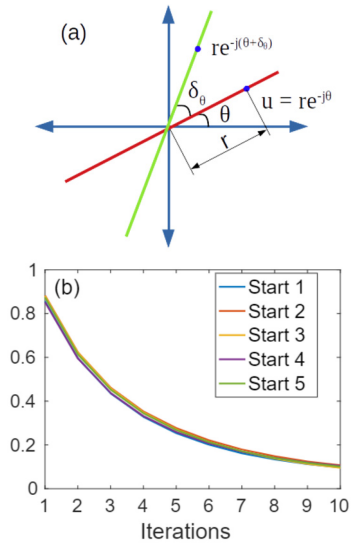


Fig. 1. (a) Red and green lines depict the nominal trajectory of a radial line and its trajectory after perturbation with $\boldsymbol{\delta}_\theta$. (b) Relative norm error between actual delta $\boldsymbol{\delta}$ and estimated delta $\boldsymbol{\delta}$ for reconstruction with db4 as *k*-space sparsifying basis, with SR = 0.5 and $\boldsymbol{\delta}_{max}$ = 2.5°.

### B. *The Proposed ARTEC Method*

In this work, we solve the problem of accelerated reconstruction of HARDI data $\boldsymbol{X}$ with unknown random perturbations $\boldsymbol{\delta}$, in the nominal trajectories of radial spokes in *k*-space, yielding the perturbed acquisition trajectories denoted as $\mathbf{u} + \boldsymbol{\delta}$. The proposed method estimates $\boldsymbol{X}$ and $\boldsymbol{\delta}$ using an alternating minimization algorithm by solving the two sub-problems. We start with a random initialization of the perturbations $\boldsymbol{\delta}$ with which we recover $\boldsymbol{X}$ by solving the HARDI reconstruction problem using the spherical ridgelets as the *q*-space sparsifying basis. The reconstruction problem is presented as a synthesis-analysis formulation:

$$\min_{\mathbf{S},\boldsymbol{\delta}} \frac{1}{2} \| \boldsymbol{\Phi}_{k,q}\mathcal{F}(\mathbf{u}+\boldsymbol{\delta})\mathbf{S}\boldsymbol{\Gamma} - \mathbf{Y} \|_F^2 + \lambda \| \boldsymbol{\Psi}\mathbf{S} \|_1, \qquad (1)$$

under the constraint $\boldsymbol{X} = \boldsymbol{S}\boldsymbol{\Gamma}$, where $\mathbf{Y} \in \mathbb{R}^{r_k \times r_q}$ is the subsampled HARDI data, $\boldsymbol{\Gamma} \in \mathbb{R}^{d_G \times d}$ is the overcomplete spherical ridgelet dictionary with $d_G$ atoms, $\boldsymbol{S}$ is the matrix with spherical ridgelet coefficients, $\boldsymbol{\Psi}$ is the *k*-space sparsifying basis, and $\mathcal{F}(\mathbf{u}+\boldsymbol{\delta})$ is the Fourier operator with *k*-space frequencies $\mathbf{u}+\boldsymbol{\delta}$. $\mathbf{u} \in \mathbb{R}^{v \times d}$ and $\boldsymbol{\delta} \in \mathbb{R}^{v \times d}$ are the nominal frequencies and frequency perturbations respectively. Further, we compared reconstruction performance with two *k*-space sparsifying bases: 1) TV penalty (or finite differences) with $l_1$ constraint as used in SAAS [3] and 2) db4 wavelet as used in MSR-HARDI [9].

1) *Update for* $\boldsymbol{S}$ *:* For the update of $\boldsymbol{S}$, we assume the perturbations $\boldsymbol{\delta}$ to be known. Further, the relation in (1) is reformulated using auxiliary linear constraint $\mathbf{Z} = \boldsymbol{\Psi}\mathbf{S}$ as:

$$\min_{\mathbf{S},\mathbf{Z}} \frac{1}{2} \| \boldsymbol{\Phi}_{k,q}\mathcal{F}(\mathbf{u}+\boldsymbol{\delta})\mathbf{S}\boldsymbol{\Gamma} - \mathbf{Y} \|_F^2 + \frac{\rho}{2} \| \mathbf{Z} - \boldsymbol{\Psi}\mathbf{S} \|_F^2 + \lambda \| \mathbf{Z} \|_1, \qquad (2)$$

which is solved using the smooth-FISTA algorithm [10].

2) *Update for* $\boldsymbol{X}$: After solving (2) for $\mathbf{S}$, $\boldsymbol{X}$ is obtained using $\boldsymbol{X} = \boldsymbol{S}\boldsymbol{\Gamma}$.

3) *Update for* $\boldsymbol{\delta}$: After estimating $\boldsymbol{X}$, we estimate values of perturbations $\boldsymbol{\delta}$ by minimizing $\| \boldsymbol{\Phi}_{k,q}\mathcal{F}(\mathbf{u}+\boldsymbol{\delta})\mathbf{X} - \mathbf{Y} \|_F^2$ and selecting the $\boldsymbol{\delta}$ that yields minimum error. Values of $\boldsymbol{\delta}$ corresponding to a specific radial line are updated independently using a linear brute force search in a grid of range $[-p, p]$, where $p$ is the magnitude of the maximum expected value of $\boldsymbol{\delta}$ in the signal and $n_p$ is the number of grid points. The alternating updation of $\boldsymbol{X}$ and $\boldsymbol{\delta}$ is performed till the convergence is achieved. The proposed alternating minimization scheme is summarized in Algorithm-1.

**Algorithm 1**: Algorithm for ARTEC

**Initialize**: converged ← False, $\epsilon = 0.0001$
  $\boldsymbol{\delta} \leftarrow$ samples from $[-p, p]$
**Choose**: $\lambda$ and $\rho$
**Input**: $\mathbf{S} = \mathbf{0}$
**while** converged == False
  #(1) Estimate **S**:
  $\min_S \frac{1}{2} \| \boldsymbol{\Phi}_{k,q}\mathcal{F}(\mathbf{u}+\boldsymbol{\delta})\mathbf{S}\boldsymbol{\Gamma} - \mathbf{Y} \|_F^2 + \lambda \| \boldsymbol{\Psi}\mathbf{S} \|_1$
  #(2) Estimate **X**:
  $\mathbf{X} = \mathbf{S}\boldsymbol{\Gamma}$
  #(3) Estimate $\boldsymbol{\delta}$ as:
  **for** $i = 1$ *to* $n_p$
    # For each value of $\boldsymbol{\delta}$ sampled
    # from Uniform $[-p, p]$, try to achieve:
    $\min_{\boldsymbol{\delta}} \frac{1}{2} \| \boldsymbol{\Phi}_{k,q}\mathcal{F}(\mathbf{u}+\boldsymbol{\delta})\mathbf{X} - \mathbf{Y} \|_F^2$
  **end**
  **if** $|| \boldsymbol{\delta}_{prev} - \boldsymbol{\delta} || < \epsilon$
    converged ← *True*
  **end**
    Return: $\boldsymbol{X}, \boldsymbol{S}, \boldsymbol{\delta}$
**end**
**Output**: Estimated $\boldsymbol{X}$ and $\boldsymbol{\delta}$

## III. Experiments and Results

To validate the method, we use one phantom HARDI from the ISBI 2013 HARDI Reconstruction Challenge[1] as well as one real HARDI image "01020-dwi-filt-Ed" from open-source NAMIC dataset[2]. The reconstruction performance is evaluated using the peak signal-to-noise ratio (PSNR).

### A. *Simulation of Trajectory Errors*

For the present work, we represent nominal frequency point $\mathrm{u} = re^{-j\theta}$, where $r$ is the radial distance of point from the origin and $\theta \in [0, \pi]$ of the radial line (Fig. 1(a)). In the nominal trajectories, we retrospectively introduced random angular perturbations $\delta_\theta$ leading to the perturbed trajectory and hence, perturbed frequency $\mathrm{u} + \delta = re^{-j(\theta+\delta_\theta)}$ as shown in Fig. 1(a) on the green color radial line. The perturbations $\delta_\theta$ are randomly chosen from a uniform distribution $[-\delta_{\theta,\max}, \delta_{\theta,\max}]$.

For both the datasets, we generated gold standard measurements $\boldsymbol{Y}$ from the available HARDI image $\boldsymbol{X}$ and known perturbations $\boldsymbol{\delta}_{true}$ using the relation $\mathbf{Y} =$

[1] http://hardi.epfl.ch/static/events/2013–ISBI

[2] http://insight-journal.org/midas/collection/view/190

$\boldsymbol{\Phi}_{k,q}\mathcal{F}(\mathbf{u}+\boldsymbol{\delta})\mathbf{X}$. Next, ARTEC is used to recover $\mathbf{X}$ after correcting for $\boldsymbol{\delta}$. We compared reconstructions for three cases:

1) **NT**: Reconstruction using only nominal trajectories $\mathbf{u}$.
2) **AT**: Reconstruction using actual trajectory $\mathbf{u}+\boldsymbol{\delta}_{true}$ considering that the true perturbations are known.
3) **CT**: Reconstruction using corrected trajectory $\mathbf{u}+\boldsymbol{\delta}$ by estimating the deviations in trajectory (i.e. $\boldsymbol{\delta}$) using ARTEC.

We varied $\lambda$ for all the experiments and chose values that yielded minimum reconstruction error. For the reconstruction with db4 at $SR = 0.5$ as depicted in Fig. 1 the value of $\lambda$ is kept as 0.05. The value of $\rho$ is increased gradually as per parameter continuation [10]. The algorithms are iterated till the error falls below a certain threshold, fixed as $\epsilon = 10^{-4}$.

### B. ARTEC Applied on HARDI Phantom Data

We selected HARDI data of dimension $50 \times 50 \times 50 \times 64$ (i.e., 64 gradient directions) with $b = 3000$ and an SNR of 30dB with magnitudes corrupted by Rician noise. In the *k*-space, the number of radial lines in each slice depends on the sampling ratio (SR), while the number of samples on each radial line is fixed to 50. In our experiments, we have shown reconstruction of the central slice of the HARDI phantom at different sampling ratios and sampling strategies. We also verified the convergence of the algorithm by reconstructing the signal at *k*-space $SR = 0.5$ using five different random initialization of $\boldsymbol{\delta}$ with $\boldsymbol{\delta}_{max} = 2.5°$ as shown in Fig. 1(b). Since ARTEC involves joint (*k*-*q*)-space reconstruction as discussed in Sec. II-B1, we first compared it with an MR reconstruction scheme, wherein each *q*-sample is reconstructed independently. We performed reconstruction of each *q*-sample with nominal trajectories (NT-S) and actual trajectories (AT-S) using db4-wavelet as *k*-space sparsifying basis following [11]. However, as evident from Fig. 2(a), reconstruction using the joint problem presented in Sec. II-B1 at nominal trajectories (NT) and actual trajectories (AT) is significantly better at all sampling ratios. Further, using the joint problem, we compared the reconstruction performance under two scenarios:

1) Identical nominal radial sampling pattern in all *q*-samples, denoted as *Same-u*. Performance is shown in Fig. 2(a-b).
2) Different nominal radial sampling pattern in *q*-samples, denoted as *Diff-u*. Performance is shown in Fig. 2(c-d).

The reconstruction comparisons are shown with db4-wavelet (ARTEC-db4) and finite-differences (ARTEC-TV) as *k*-space sparsifying basis, respectively with *k*-space sampling ratios varying from 10% to 90%. For all the cases, we observed that the reconstruction with CT is comparable to that of AT at all sampling ratios while also depicting a significant gain over NT. We can also observe that the reconstruction using *Diff-u* sampling scheme is significantly better than the *Same-u* indicating that each *q*-sample should be acquired using a different sampling pattern. This is also evident from the respective qualitative comparisons of ARTEC-db4 and ARTEC-TV using NT, AT, and CT at $SR = \{0.2, 0.5\}$, and $\boldsymbol{\delta}_{max} = 2.5°$ with the two sampling schemes as shown in Figs. 3 and 4. We observe that the reconstruction with CT is comparable to that with AT and has significant improvement over NT. Henceforth, *Diff-u* is followed for all our experiments.

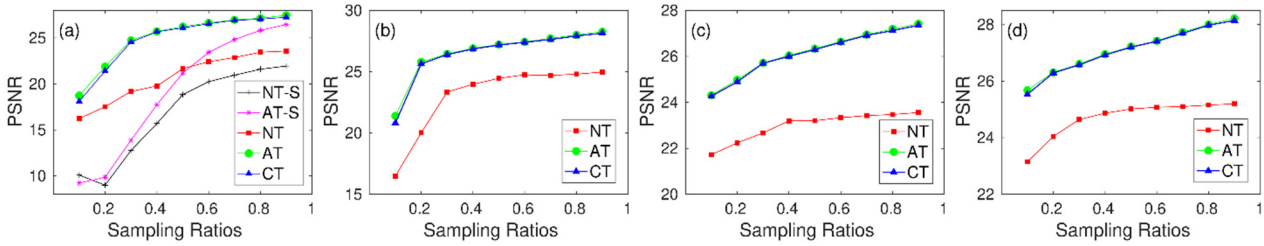


Fig. 2. (a-b) Reconstruction using *Same-u* scheme: (a) Reconstruction using ARTEC-db4 and (b) Reconstruction using ARTEC-TV. (c-d) Reconstruction using *Diff-u* scheme: (c) Reconstruction using ARTEC-db4 and (d) Reconstruction using ARTEC-TV.

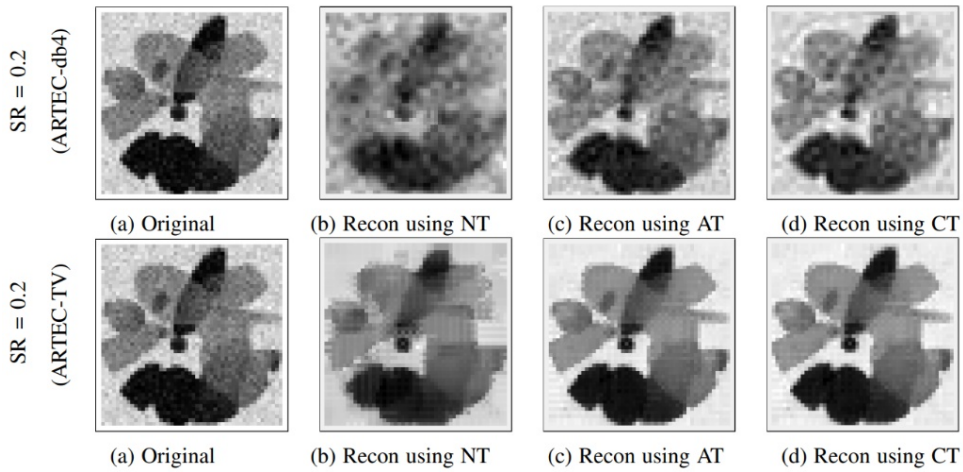


Fig. 3. Reconstruction using *Same-u* scheme: (a) One *b*=3000 image from original central slice of HARDI phantom dataset. (b-c-d) images reconstructed with ARTEC-db4 and ARTEC-TV using NT, AT and CT; *k*-space sampling ratio (SR) is 0.2 and $\delta_{max}$ = 2.5°. 'Recon' denotes reconstruction.

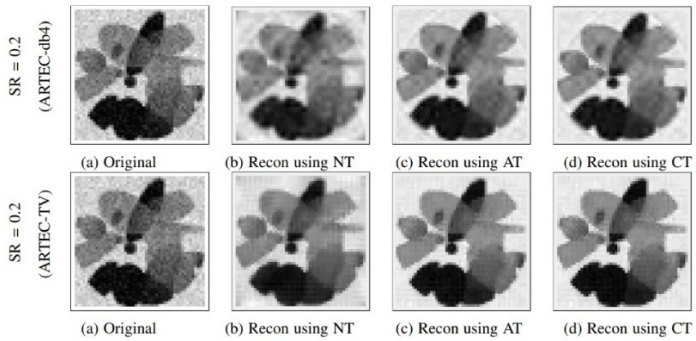


Fig. 4. Reconstruction using *Diff-u* scheme: (a) One b=3000 image from original central slice of HARDI phantom dataset. (b-c-d) images reconstructed with ARTEC-db4 and ARTEC-TV using NT, AT and CT; *k*-space sampling ratio (SR) is 0.2 and $\delta_{max}$ = 2.5°. 'Recon' denotes reconstruction.

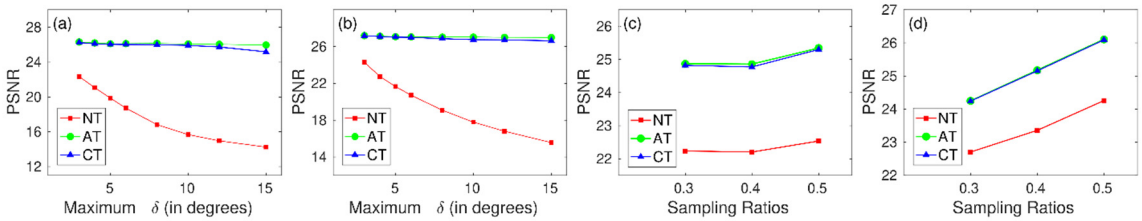


Fig. 5. PSNR with Diff-u scheme
(a-b) Reconstruction over different values of $\delta_{\max}$ keeping *k*-space SR = 0.5: (a) using ARTEC-db4 and (b) using ARTEC-TV;
(c-d) Reconstruction over different values of (*k*-*q*)-space subsampling with $\delta_{\max}$ = 2.5° and SR =0.3 (30% subsampling in both *k*-space and *q*-space yields an effective sampling ratio of 0.09): (c) using ARTEC-db4 and (d) using ARTEC-TV.

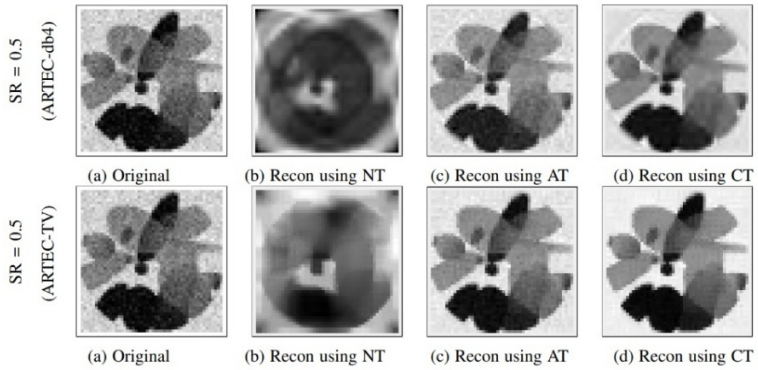


Fig. 6. Quality of reconstructed images using Diff-u scheme with *k*-space sampling ratio (SR) = 0.2 and $\delta_{max}$ = 15°
(a) Original central slice of HARDI phantom dataset at *b*=3000; (b-c-d) Central slice reconstructed using ARTEC-db4 and ARTEC-TV with NT, AT and CT; 'Recon' implies reconstruction.

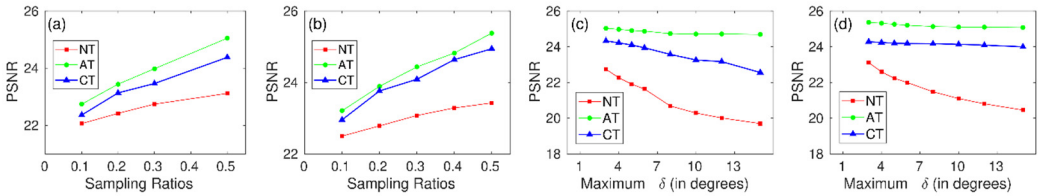


Fig. 7. PSNR with Diff-u scheme
(a-b) Reconstruction over different values of *k*-space sampling ratios and $\delta_{max}$ = 2.5°: (a) using ARTEC-db4 and (b) using ARTEC-TV;
(c-d) Reconstruction over different values of $\delta_{max}$ and SR = 0.5: (c) using ARTEC-db4 and (d) using ARTEC-TV.

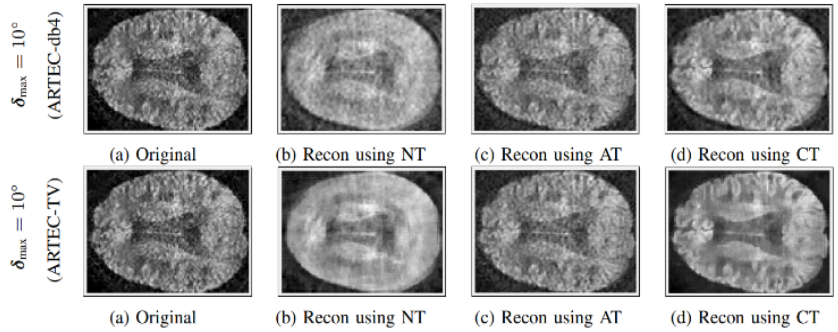


Fig. 8. Quality of reconstructed images using Diff-u scheme with *k*-space sampling ratio (SR) = 0.5 and $\delta_{max}$ = 10°
(a) Original slice selected from the corpus callosum region of real HARDI dataset; (b-c-d) Slice reconstructed using ARTEC-db4 and ARTEC-TV with NT, AT and CT; 'Recon' implies reconstruction

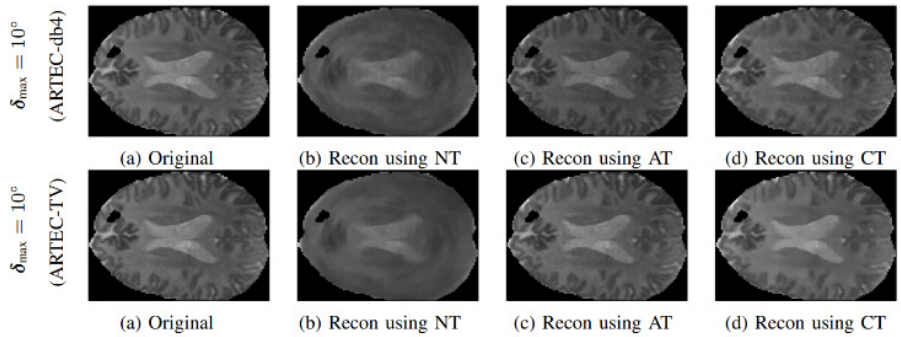


Fig. 9. Quality of mean diffusivity (MD) maps of images reconstructed with *k*-space sampling ratio (SR) = 0.5 and $\delta_{max}$ = 10° (a) MD map of original slice selected from the corpus callosum region of real HARDI dataset; (b-c-d) MD map of slice reconstructed using ARTEC-db4 and ARTEC-TV with NT, AT and CT; 'Recon' implies reconstruction

Next, for comparison on different amounts of perturbations, we reconstructed the phantom slice at SR = 0.5 with $\boldsymbol{\delta}_{max}$varying from 2.5° to 15° as shown in Fig. 5(a-b). In Fig. 6, reconstruction performance is shown with ARTEC-db4 and ARTEC-TV at $SR = 0.5$, and $\boldsymbol{\delta}_{max}$ = 15°. We observe that even at high perturbation error of $\boldsymbol{\delta}_{max}$ = 15°, the reconstruction with the corrected trajectory (CT) is comparable to that of actual trajectory (AT), and has significant improvement over NT. We also tested the reconstruction of ARTEC-db4 and ARTEC-TV at different joint (*k*-*q*)-space sampling ratios. We observed comparable results with AT and CT that further establishes the robustness of the ARTEC method as shown in Fig. 5(c-d).

### *A. ARTEC Applied on Real HARDI Data*

We used a real HARDI brain volume of size 144×144×85×59(i.e., with 59 gradient directions). For better representation, we selected an axial slice from the corpus callosum region of the brain. From Fig. 7(a-b), we observe that both ARTEC-db4 and ARTEC-TV significantly improve reconstruction using CT over NT, while it is comparable to that with AT. A similar trend continues for reconstruction at different $\boldsymbol{\delta}_{max}$ as shown in Fig. 7(c-d). Also, in Fig. 8, we observe significantly improved reconstruction of ARTEC-db4 using CT compared to NT. These results indicate better visualization of brain structure compared to the original image perhaps owing to the inherent denoising property of the compressing sensing framework. Further, since ARTEC (with CT) has to estimate trajectory perturbations, which requires the signal to be reconstructed multiple times, it might have also led to denoising. Similarly, we observed improved results on the mean diffusivity maps of the real HARDI image reconstructed using ARTEC methods as shown in Fig. 9.

## IV. Conclusions and Future Scope

In this work, we presented a joint framework, ARTEC, for the accelerated reconstruction of the HARDI signal undersampled in the joint (*k*-*q*)-space while incorporating trajectory error corrections. We validated ARTEC on reconstruction performance at different sampling ratios with subsampling introduced only in the *k*-space and in the joint (*k*-*q*)-space, and over a wide range of induced perturbations. ARTEC satisfactorily estimated the induced perturbations. The signal reconstruction performance with unknown perturbation is comparable to the case if the perturbations were known.

## Conflict of Interest

The authors declare no conflict of interest.

## Author Contributions

Ashutosh, Anubha and Ajit conceived the presented methodology and planned the experiments. Ashutosh performed the computations. Ashutosh, Anubha, and Ajit discussed and interpreted the results and contributed to writing the draft. All authors approved the final version.

## References

[1] P. J. Basser, J. Mattiello, R. Turner, and D. L. Bihan, "Diffusion tensor echo-planar imaging of human brain," in *Proc. the SMRM*, 1993, vol. 584.

[2] O. Michailovich and Y. Rathi, "On approximation of orientation distributions by means of spherical ridgelets," *IEEE Transactions on Image Processing*, vol. 19, no. 2, pp. 461–477, 2010.

[3] E. Schwab, R. Vidal, and N. Charon, "Joint spatial-angular sparse coding for dMRI with separable dictionaries," *Medical Image Analysis*, vol. 48, pp. 25–42, 2018.

[4] K. E. Jeong, E. W. Hsu, and E.-K. Jeong, "Diffusion MRI using two-dimensional single-shot radial imaging (2D ss-rDWI) with variable flip angle and random view ordering," *Magnetic Resonance Imaging*, vol. 61, pp. 273–284, 2019.

[5] K. L. Wright, J. I. Hamilton, M. A. Griswold, V. Gulani, and N. Seiberlich, "Non-cartesian parallel imaging reconstruction," *Journal of Magnetic Resonance Imaging*, vol. 40, no. 5, pp. 1022–1040, 2014.

[6] A. Moussavi and S. Boretius, "Imperfect magnetic field gradients in radial *k*-space encoding—quantification, correction, and parameter dependency," *Magnetic Resonance in Medicine*, vol. 81, no. 2, pp. 962–975, 2019.

[7] J. D. Ianni and W. A. Grissom, "Trajectory auto-corrected image reconstruction," *Magnetic resonance in Medicine*, vol. 76, no. 3, pp. 757–768, 2016.

[8] J. Cheng, D. G. Shen, P.-T. Yap, and P. J. Basser, "Single-and multiple-shell uniform sampling schemes for diffusion MRI using spherical codes," *IEEE Transactions on Medical Imaging*, vol. 37, no. 1, pp. 185–199, 2017.

[9] A. Vaish, A. Gupta, and A. Rajwade, "MSR-HARDI: Accelerated reconstruction of HARDI data using multiple sparsity regularizers," in *Proc. 2020 IEEE International Conference on Image Processing (ICIP)*, 2020, pp. 2850–2854.

[10] Z. Tan *et al*., "Smoothing and decomposition for analysis sparse recovery," *IEEE Transactions on Signal Processing*, vol. 62, no. 7, pp. 1762–1774, April 2014.

[11] H. Pandotra, E. Malhotra, A. Rajwade, and K. S. Gurumoorthy, "Dealing with frequency perturbations in compressive reconstructions with fourier sensing matrices," *Signal Processing*, vol. 165, pp. 57–71, 2019.